5-1-2019

Absolute Dimensions of the Early F-type Eclipsing Binary V506 Ophiuchi

Guillermo Torres
Harvard-Smithsonian Center for Astrophysics

Claud H. Sandberg Lacy
University of Arkansas, Fayetteville

Francis C. Fekel
Tennessee State University

Matthew W. Muterspaugh
Columbia State Community College

The Astrophysical Journal, 876:41 (7pp), 2019 May 1 https://doi.org/10.3847/1538-4357/ab1487

Absolute Dimensions of the Early F-type Eclipsing Binary V506 Ophiuchi

Guillermo Torres[1], Claud H. Sandberg Lacy[2], Francis C. Fekel[3], and Matthew W. Muterspaugh[3,4]
[1] Center for Astrophysics | Harvard & Smithsonian, 60 Garden Street, Cambridge, MA 02138, USA; gtorres@cfa.harvard.edu
[2] Physics Department, University of Arkansas, Fayetteville, AR 72701, USA
[3] Center of Excellence in Information Systems, Tennessee State University, Nashville, TN 37209, USA
[4] College of Life and Physical Sciences, Tennessee State University, Nashville, TN 37209, USA
Received 2019 February 14; revised 2019 March 20; accepted 2019 March 21; published 2019 May 1

Abstract

We report extensive differential *V*-band photometry and high-resolution spectroscopic observations of the early F-type, 1.06-day detached eclipsing binary V506 Oph. The observations, along with times of minimum light from the literature, are used to derive a very precise ephemeris and the physical properties for the components, with the absolute masses and radii being determined to 0.7% or better. The masses are $1.4153 \pm 0.0100\ M_{\odot}$ and $1.4023 \pm 0.0094\ M_{\odot}$ for the primary and secondary, the radii are $1.725 \pm 0.010\ R_{\odot}$ and $1.692 \pm 0.012\ R_{\odot}$, and the effective temperatures are 6840 ± 150 K and 6780 ± 110 K, respectively. The orbit is circular and the stars are rotating synchronously. The accuracy of the radii and temperatures is supported by the resulting distance estimate of 564 ± 30 pc, which is in excellent agreement with the value implied by the trigonometric parallax listed in the *Gaia*/Data Release 2 catalog. Current stellar evolution models from the Modules for Experiments in Stellar Astrophysics (MESA) Isochrones and Stellar Tracks series for a composition of $[\mathrm{Fe/H}] = -0.04$ match the properties of both stars in V506 Oph very well at an age of 1.83 Gyr and indicate they are halfway through their core hydrogen-burning phase.

Key words: binaries: eclipsing – stars: evolution – stars: fundamental parameters – stars: individual (V506 oph) – techniques: photometric – techniques: spectroscopic

Supporting material: machine-readable tables

1. Introduction

The variability of V506 Oph (TYC 993-1631-1, *Gaia*/Data Release 2 (DR2) 4486661994344201344, and $V = 11.1$, SpT F1 V) was discovered photographically by Hoffmeister (1935), who classified it as an Algol-type eclipsing system. The binary orbital period of 1.06 days was first established by Soloviev (1937). Aside from the many times of minimum light measured since, charge coupled device (CCD) light curves have been reported occasionally in the more recent literature (Pojmanski & Maciejewski 2004; Lapham & Snyder 2007; Kochanek et al. 2017), sometimes only in graphical form, but there is no detailed study of the system as yet.

Here, we report extensive new photometric observations of V506 Oph as well as radial velocity measurements, which we combine to determine the physical properties of the system for the first time. The spectroscopic observations and velocity measurements are presented in Section 2. In Section 3, we combine them with times of minimum light from the literature to derive an accurate linear ephemeris as well as the spectroscopic elements. The photometric observations are reported in Section 4 and are subjected to a detailed light-curve analysis in Section 5. The physical properties of the stars, derived in Section 6, are then compared with predictions from recent stellar evolution models in Section 7. Final remarks are given in Section 8.

2. Spectroscopy

V506 Oph was observed spectroscopically with two different instruments. Between 2010 May and 2017 February, we monitored the binary with the Center for Astrophysics|Harvard & Smithsonian (CfA) Tillinghast Reflector Echelle Spectrograph (Szentgyorgyi & Fűrész 2007; Fűrész 2008) attached to the 1.5 m Tillinghast reflector at the Fred L. Whipple Observatory on Mount Hopkins, Arizona. This bench-mounted, fiber-fed instrument delivers spectra with a resolving power of $R \approx 44{,}000$ covering the wavelength range 3900–9100 Å in 51 orders. We gathered 48 spectra with signal-to-noise ratios (S/N) near the Mg I b triplet (5187 Å) ranging from 21 to 74 per resolution element of 6.8 km s^{-1}. Wavelength calibrations relied on exposures of a Thorium-Argon lamp taken before and after each science frame, and the reductions were performed with a dedicated pipeline.

Radial velocities from the CfA spectra were measured with the two-dimensional cross-correlation technique TODCOR (Zucker & Mazeh 1994). Templates appropriate for each star were taken from a library of precomputed synthetic spectra based on model atmospheres by R. L. Kurucz (see Nordström et al. 1994; Latham et al. 2002). For this analysis, we used only the 100 Å wide order centered on the Mg I b triplet, as previous experience indicates it contains most of the velocity information and because our synthetic templates are limited in coverage to a narrow region surrounding that feature. We selected the best templates by running grids of cross-correlations over wide ranges in the effective temperature ($T_{\rm eff}$) and rotational broadening ($v \sin i$ when seen in projection) at a fixed solar metallicity and values of the surface gravity of $\log g = 4.0$, close to our final determinations in Section 6. Following Torres et al. (2002) we selected the template parameters giving the highest cross-correlation value averaged over all observations, with weights set by the strength of each exposure. In this way, we estimated the temperatures to be 6840 ± 150 K and 6860 ± 150 K for the primary (the marginally more massive star) and secondary, which are the same within their uncertainties. They correspond approximately to spectral type F1. The uncertainties are based on the scatter from the individual spectra, with an extra 100 K added

Table 1
Heliocentric Radial Velocity Measurements of V506 Oph from CfA

HJD (2,400,000+)	RV_1 (km s^{-1})	σ_1 (km s^{-1})	RV_2 (km s^{-1})	σ_2 (km s^{-1})	Orbital Phase
55338.8444	122.23	3.66	−134.06	3.90	0.0881
55347.7766	−149.05	2.70	146.47	2.88	0.5113
55369.9595	−124.82	4.73	127.38	5.05	0.4302
55381.6768	−148.08	3.01	142.72	3.21	0.4798
55640.9437	138.89	2.73	−142.29	2.91	0.9725
55758.7037	140.27	2.25	−148.18	2.41	0.0220
56019.0159	−147.43	4.21	148.12	4.49	0.5005
56027.9888	139.07	2.50	−147.22	2.67	0.9621
56058.8175	141.14	3.92	−146.90	4.18	0.0341
56074.7773	119.63	1.80	−128.91	1.92	0.0844
56135.7569	−124.63	2.70	128.16	2.88	0.5891
56205.5940	−143.66	2.95	135.05	3.15	0.4466
56351.0042	−137.24	2.81	133.00	3.00	0.5707
56375.9216	129.97	2.84	−133.45	3.03	0.0682
56401.9332	−121.29	2.82	116.96	3.02	0.5975
56404.9811	−150.90	2.42	139.02	2.58	0.4718
56435.8296	−141.08	2.18	133.32	2.33	0.5624
56436.8014	−150.41	2.44	146.09	2.60	0.4788
56460.7272	139.48	4.62	−147.98	4.93	0.0412
56502.6813	−120.78	3.66	119.43	3.90	0.6046
56554.6252	−125.01	1.98	122.39	2.11	0.5885
56739.0051	−154.96	3.74	142.25	3.99	0.4616
56761.9152	135.28	4.07	−137.51	4.34	0.0662
56795.7617	142.51	3.36	−148.01	3.59	0.9840
56816.9153	132.73	3.14	−138.07	3.36	0.9322
56824.8427	−130.78	2.82	124.13	3.01	0.4078
57063.0212	143.69	3.75	−146.77	4.00	0.0139
57086.9575	−127.83	2.65	125.97	2.83	0.5862
57089.0347	−147.38	4.46	140.41	4.76	0.5450
57091.0266	−131.47	3.32	123.07	3.55	0.4234
57114.0118	118.77	4.23	−122.62	4.52	0.0988
57118.0005	85.33	3.24	−102.77	3.46	0.8602
57141.9453	−144.11	3.95	135.13	4.22	0.4405
57168.9740	127.31	3.60	−138.77	3.84	0.9290
57207.7905	−145.52	3.50	140.23	3.74	0.5336
57291.6177	−123.53	3.82	114.85	4.08	0.5840
57443.0342	−108.50	2.83	94.27	3.02	0.3721
57447.0052	105.52	2.49	−113.92	2.66	0.1168
57472.9373	−130.44	3.86	132.20	4.12	0.5712
57498.8922	136.32	2.60	−141.82	2.77	0.0471
57514.8946	93.96	4.26	−99.61	4.55	0.1376
57523.9009	−106.32	3.84	99.23	4.09	0.6307
57534.8209	125.13	3.13	−134.26	3.34	0.9284
57558.6875	−141.76	3.13	133.24	3.34	0.4350
57581.6919	99.09	2.36	−108.41	2.52	0.1285
57585.7499	134.28	3.77	−143.35	4.03	0.9552
57598.6716	87.23	2.89	−100.39	3.09	0.1406
57807.0186	−112.31	3.77	101.98	4.03	0.6151

Note. Phases are calculated from the reference time of primary eclipse in Table 4.

in quadrature, to be conservative. The rotational velocities were determined to be 80 ± 3 km s^{-1} for both stars. Thus, the spectroscopic properties are essentially identical. The light ratio at the mean wavelength of our observations (see Zucker & Mazeh 1994) was found to be $\ell_2/\ell_1 = 0.96 \pm 0.03$. The resulting radial velocities in the heliocentric frame are listed in Table 1 along with their uncertainties.

V506 Oph was also observed at the Fairborn Observatory in southeast Arizona near Washington Camp, between 2012 February and 2018 May. For this, we used the Tennessee State University 2 m Astronomical Spectroscopic Telescope (AST) and a fiber-fed echelle spectrograph (Eaton & Williamson 2007). The detector was a Fairchild 486 CCD with 4K × 4K pixels 15 μm in size, which results in echelle spectra that have 48 orders and cover a wavelength range of 3800–8260 Å (Fekel et al. 2013). Because of the faintness of the system, we used a fiber diameter that produced a spectral resolution of 0.4 Å, but even so, given the weakness and very significant line broadening of the features, many of the spectra did not have a high enough S/N to provide meaningful results. However, we were able to obtain useful velocity measurements from 17 AST spectra that had a resolving power of 15000 at 6000 Å and an average S/N of about 40.

Table 2
Heliocentric Radial Velocity Measurements of V506 Oph from the Fairborn Observatory

HJD (2,400,000+)	RV_1 (km s^{-1})	RV_2 (km s^{-1})	Orbital Phase
55976.9665	82.80	−92.80	0.5980
56419.9033	−144.60	137.40	0.2945
56454.8887	−147.90	140.10	0.2863
56565.6922	138.30	−149.00	0.7757
56731.9907	80.20	−92.60	0.5979
56769.8765	−140.30	130.50	0.3248
56799.8553	79.40	−94.00	0.5953
56902.7375	92.80	−102.00	0.6149
57088.9577	−150.00	142.40	0.2235
57174.7409	−108.70	98.60	0.1184
57509.8563	−123.30	113.10	0.1376
57541.8116	−145.70	145.20	0.2720
57595.7453	−110.80	104.20	0.1323
57653.6778	146.00	−149.70	0.7636
57851.8666	120.80	−126.50	0.6588
58003.6971	116.70	−129.90	0.8374
58245.8184	−129.50	121.30	0.1616

Note. Velocity uncertainties are estimated to be 3.2 and 2.6 km s^{-1} for the primary and secondary, respectively. Phases are calculated from the reference time of primary eclipse in Table 4.

A description of the general radial velocity reduction of the Fairborn AST spectra has been given by Fekel et al. (2009). In particular for V506 Oph, we used a solar line list that consisted of 168 mostly neutral Fe lines that cover a wavelength range of 4920–7100 Å. The individual lines were fitted with a rotational broadening function (Sandberg Lacy & Fekel 2011). Unpublished velocities of several IAU solar-type radial velocity standards show that velocities obtained with our Fairchild CCD have a −0.6 km s^{-1} offset relative to the velocities of Scarfe (2010). Thus, 0.6 km s^{-1} has been added to each velocity. We list these measurements in Table 2. We estimate the uncertainties to be 3.2 and 2.6 km s^{-1} for the primary and secondary, respectively, from the scatter of a preliminary spectroscopic orbital solution.

Rotational broadening fits of the stellar lines in our 17 spectra result in $v \sin i$ values of 81 ± 3 km s^{-1} for both components. From the same spectra, the average equivalent width ratio of the secondary to the primary, which should be equivalent to the light ratio since the spectra appear to be very similar, is $\ell_2/\ell_1 = 0.96 \pm 0.03$, which is the same as obtained from the CfA spectra.

Table 3
Times of Minimum Light for V506 Oph

HJD (2,400,000+)	σ (days)	Eclipse	Type	Year	$(O-C)$ (days)	Source
25502.313	⋯	2	pg	1928.6990	0.01250	1
26068.578	⋯	2	pg	1930.2494	0.00928	1
26145.469	⋯	1	pg	1930.4599	0.01929	1
26592.424	⋯	2	pg	1931.6836	0.00415	1
26856.481	⋯	2	pg	1932.4065	0.01473	1

Note. The uncertainties in the second column are taken directly from the original publications. Scale factors for these errors determined from our joint solution with the spectroscopy are given in the text. The "Eclipse" column refers to the primary (1) or secondary (2) minimum. "Type" is "pg," "v," or "pe" for photographic, visual, or photoelectric/CCD observations. Sources are: (1) https://www.bav-astro.eu/index.php/veroeffentlichungen/service-for-scientists/lkdb-engl; (2) http://var2.astro.cz/ocgate/?lang=en; (3) Lapham & Snyder (2007), with the unrealistically small formal uncertainties multiplied by 30; and (4) Lacy (2007).

(This table is available in its entirety in machine-readable form.)

Table 4
Spectroscopic Orbital Elements of V506 Oph

Parameter	Value
Adjusted Elements	
P (days)	1.060427381 ± 0.000000024
γ (km s^{-1})	−3.88 ± 0.43
K_1 (km s^{-1})	146.76 ± 0.44
K_2 (km s^{-1})	148.11 ± 0.45
Min I (HJD − 2,400,000)	53,123.782733 ± 0.000037
ΔRV_{CfA} (km s^{-1})	−0.99 ± 0.65
$\Delta RV_{Fairborn}$ (km s^{-1})	−0.98 ± 1.03
ΔRV (km s^{-1})	+1.02 ± 0.91
Derived Quantities	
$M_1 \sin^3 i$ ($M_\odot^N$)	1.4151 ± 0.0096
$M_2 \sin^3 i$ ($M_\odot^N$)	1.4022 ± 0.0094
$q \equiv M_2/M_1$	0.9909 ± 0.0042
$a_1 \sin i$ (10^6 km)	2.1401 ± 0.0064
$a_2 \sin i$ (10^6 km)	2.1598 ± 0.0066
$a \sin i$ ($R_\odot^N$)	6.181 ± 0.013
CfA σ_1, σ_2 (km s^{-1})	2.91, 3.26
CfA $N_{RV,1}$, $N_{RV,2}$	48, 48
Fairborn σ_1, σ_2 (km s^{-1})	3.20, 2.60
Fairborn $N_{RV,1}$, $N_{RV,2}$	17, 17
$N_{Min\ I}$, $N_{Min\ II}$	84, 92

Note. Δ_{CfA} and $\Delta_{Fairborn}$ represent the primary minus secondary velocity offsets, and ΔRV represents the global CfA minus Fairborn shift. The minimum masses and semimajor axis are expressed in units of the nominal solar mass and radius ($M_\odot^N$, $R_\odot^N$) as recommended by 2015 IAU Resolution B3 (see Prša et al. 2016).

3. Times of Minimum and Spectroscopic Orbit

Times of minimum light for V506 Oph have been recorded since 1928 by photographic, visual, and photoelectric/CCD techniques. We collect all 176 measurements that we are aware of (84 for the primary and 92 for the secondary) in Table 3, with their uncertainties when published.

Independent spectroscopic orbital solutions from the CfA and Fairborn velocities gave elements consistent with each other, except for a minor difference in the center-of-mass velocities that is of no consequence and is likely due to instrumental shifts. We, therefore, combined these data sets. Furthermore, as the times of minimum light spanning nearly 87 years constrain the ephemeris far better than our radial velocities can, we used the two kinds of observations together in a joint orbital solution to derive the final ephemeris and spectroscopic elements simultaneously. For the times of minimum without published uncertainties, we adopted errors of 0.0175, 0.0146, and 0.0035 days for the photographic,

Table 5
URSA Observations of V506 Oph

HJD (2,400,000+)	ΔV (mag)
52831.60573	1.211
52831.60763	1.232
52831.60954	1.250
52831.61143	1.305
52831.61329	1.296

(This table is available in its entirety in machine-readable form.)

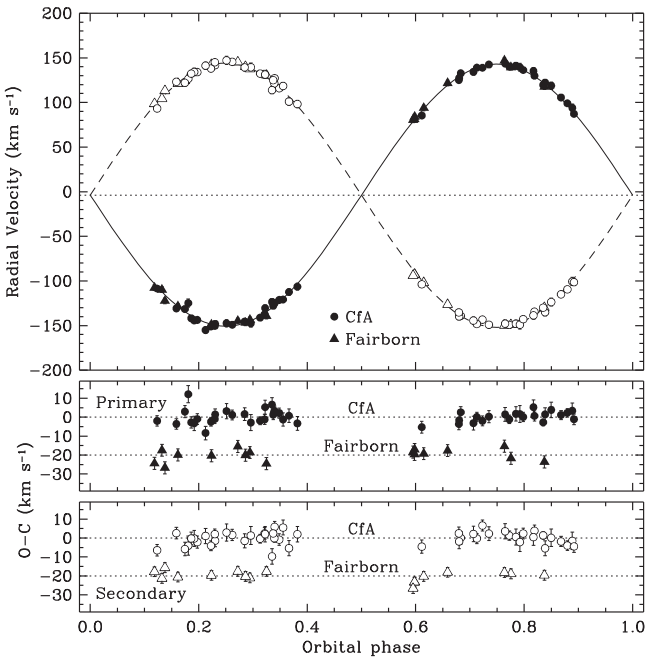

Figure 1. Radial velocity observations along with our joint spectroscopic orbital solution incorporating the times of minimum light. The dotted line marks the center-of-mass velocity of the system. Residuals are shown at the bottom, with the ones from the Fairborn Observatory displaced vertically for clarity. Phases are counted from the reference time of the primary eclipse in Table 4.

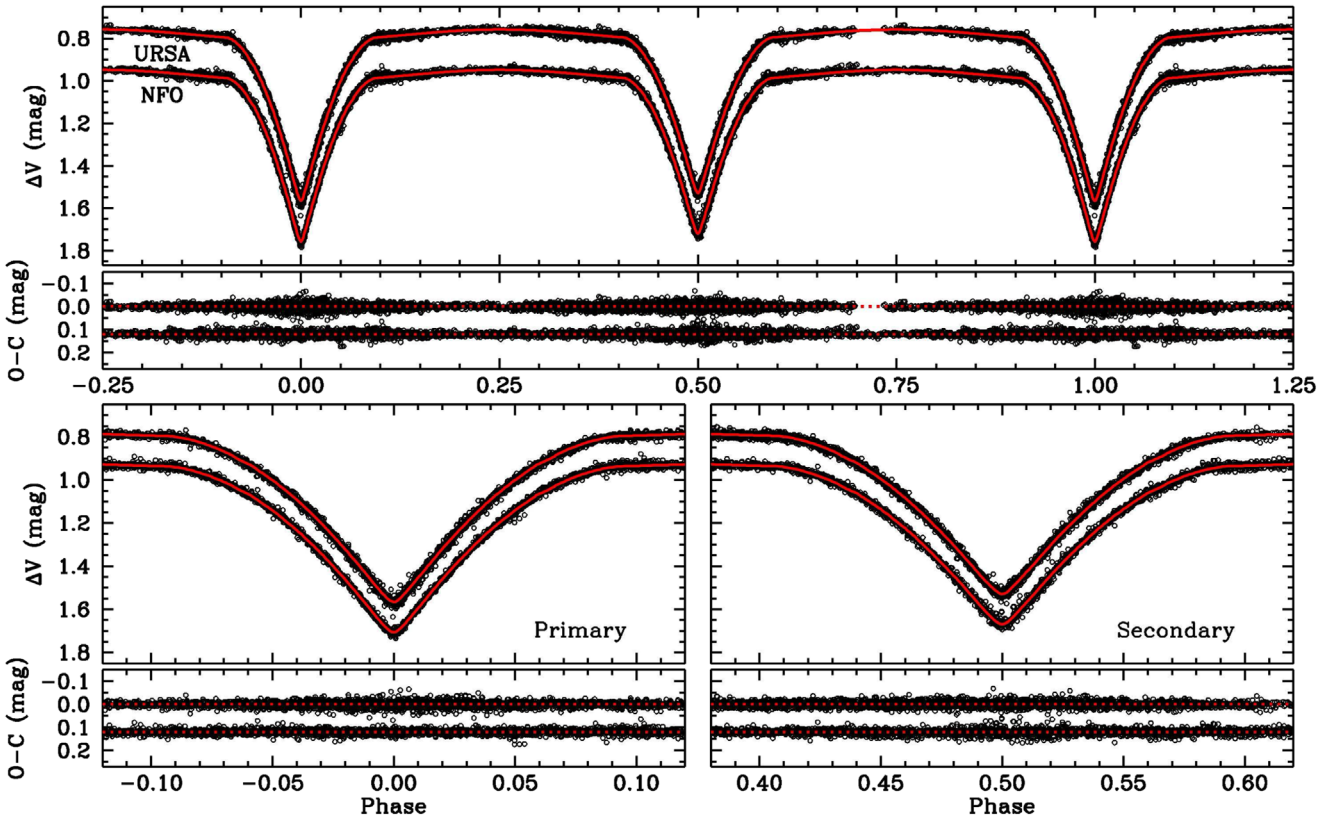

Figure 2. Photometric observations of V506 Oph from the URSA and NFO telescopes, along with the residuals. NFO is displaced vertically for clarity. Enlargements of the minima are shown at the bottom. Our adopted model discussed in Section 5 is overplotted.

Table 6
NFO Observations of V506 Oph

HJD (2,400,000+)	ΔV (mag)
53399.02069	0.960
53399.02460	0.923
53399.02849	0.911
53399.03236	0.884
53399.03625	0.862

(This table is available in its entirety in machine-readable form.)

visual, and photoelectric/CCD measurements, respectively, determined by iterations so as to achieve reduced χ^2 values near unity for each type of observation. In a similar manner, we determined appropriate scaling factors to be applied to the published visual errors of 1.09 and 1.28 for the primary and secondary measurements, and scale factors for the photoelectric/CCD errors of 1.17 and 1.65. Initial fits allowing for separate epochs of primary and secondary minimum showed no evidence of eccentricity, so the final fit assumed none. We also allowed for possible velocity offsets between the primary and secondary stars separately for the CfA and Fairborn data (ΔRV_{CfA}, $\Delta RV_{Fairborn}$), which in the case of the CfA data may result from template mismatch. We additionally solved for a systematic offset between the CfA and Fairborn velocity zero points (ΔRV), to account for possible instrumental shifts as indicated above. The results are listed in Table 4 and shown graphically in Figure 1 together with the observations and residuals.

4. Photometry

Differential photometry of V506 Oph in the V band was performed with the URSA WebScope at the University of Arkansas at Fayetteville and with the NFO WebScope near Silver City, New Mexico (see Lacy et al. 2014 for technical details). V506 Oph (var) was measured along with two nearby comparison stars (comp; TYC 993-762-1, $V = 11.30$, $B - V = 2.08$, and TYC 993-0780-1, $V = 10.78$, $B - V = 0.49$). Differential magnitudes were measured with the application `Measure` written by Lacy. The two comparison star fluxes were combined and the differential magnitudes were calculated as var−comps. We obtained 8345 URSA images between 2003 July and 2012 June on a total of 129 nights and 7475 NFO images between 2005 January and 2013 June on a total of 234 nights. Exposures were 120 sec long, and square photometric apertures with sizes of 30″ and 22″ were used for URSA and NFO, respectively. The *Gaia*/DR2 catalog lists seven nearby stars within 30″ of V506 Oph, but they are all at least eight magnitudes fainter and, therefore, do not contaminate the photometry.

Examination of the raw data revealed that the NFO measurements suffer from small systematic errors typically less than 0.02 mag, caused by imprecise centering from night to night and variations in responsivity across the field of view (see Lacy et al. 2014). We corrected this by applying nightly offsets based on a preliminary light-curve solution using the URSA data alone, which shows no such effects for V506 Oph. The full data sets are given in Table 5 (URSA) and Table 6 (NFO, including corrections). The resultant light curves are displayed in Figure 2.

Table 7
Light-curve Elements of V506 Oph from Our Combined URSA+NFO Solution

Parameter	Primary	Secondary
Adjusted Elements		
i (deg)	$89.27^{+0.18}_{-0.16}$	
$T_{\rm eff}$ (K)	6840 (fixed)	6781^{+110}_{-110}
Φ	$4.629^{+0.019}_{-0.021}$	$4.678^{+0.029}_{-0.027}$
x	$0.462^{+0.048}_{-0.048}$	$0.455^{+0.052}_{-0.052}$
β	$0.47^{+0.12}_{-0.13}$	$0.42^{+0.16}_{-0.16}$
$\Delta\phi_{\rm URSA}$	$-0.000029^{+0.000027}_{-0.000030}$	
$\Delta\phi_{\rm NFO}$	$-0.000039^{+0.000031}_{-0.000031}$	
$m_{0,\rm URSA}$ (mag)	$0.75675^{+0.00057}_{-0.00054}$	
$m_{0,\rm NFO}$ (mag)	$0.74756^{+0.00054}_{-0.00053}$	
$\ln f_{\rm URSA}$	$-0.6172^{+0.0079}_{-0.0079}$	
$\ln f_{\rm NFO}$	$-0.7513^{+0.0083}_{-0.0083}$	
Derived Quantities		
$r_{\rm pole}$	$0.2723^{+0.0016}_{-0.0014}$	$0.2673^{+0.0016}_{-0.0017}$
$r_{\rm point}$	$0.2911^{+0.0021}_{-0.0018}$	$0.2848^{+0.0021}_{-0.0022}$
$r_{\rm side}$	$0.2780^{+0.0017}_{-0.0015}$	$0.2726^{+0.0017}_{-0.0018}$
$r_{\rm back}$	$0.2863^{+0.0019}_{-0.0017}$	$0.2804^{+0.0019}_{-0.0020}$
$r_{\rm vol}$	$0.2791^{+0.0017}_{-0.0015}$	$0.2737^{+0.0017}_{-0.0018}$
$r_1 + r_2$	$0.5529^{+0.0010}_{-0.0010}$	
r_2/r_1	$0.981^{+0.011}_{-0.012}$	
$(\ell_2/\ell_1)_V$	$0.930^{+0.014}_{-0.015}$	
$\Delta T_{\rm eff}$ (K)	59^{+23}_{-24}	
$\sigma_{\rm URSA}$, $\sigma_{\rm NFO}$ (mag)	0.01079, 0.00944	
$N_{\rm URSA}$, $N_{\rm NFO}$	8345, 7475	

Note. The parameter values listed correspond to the mode of the posterior distributions, and the uncertainties are the 16% and 84% (1σ) credible intervals.

Table 8
Physical Properties of V506 Oph

Parameter	Primary	Secondary
M ($\mathcal{M}_\odot^{\rm N}$)	1.4153 ± 0.0100	1.4023 ± 0.0094
R ($\mathcal{R}_\odot^{\rm N}$)	1.725 ± 0.010	1.692 ± 0.012
$q \equiv M_2/M_1$	0.9909 ± 0.0042	
a ($\mathcal{R}_\odot^{\rm N}$)	6.182 ± 0.013	
$\log g$ (cgs, dex)	4.1155 ± 0.0061	4.1284 ± 0.0067
$T_{\rm eff}$ (K)	6840 ± 150	6780 ± 110
L ($L_\odot$)	5.84 ± 0.52	5.42 ± 0.36
$M_{\rm bol}$ (mag)	2.816 ± 0.096	2.896 ± 0.072
$\rm BC_V$ (mag)	+0.025 ± 0.100	+0.023 ± 0.100
M_V (mag)	2.79 ± 0.14	2.87 ± 0.13
$v_{\rm sync} \sin i$ (km s^{-1})[a]	82.3 ± 0.5	80.7 ± 0.6
$v \sin i$ (km s^{-1})[b]	80.5 ± 2.1	80.5 ± 2.1
$E(B-V)$ (mag)	0.088 ± 0.020	
A_V (mag)	0.273 ± 0.062	
Dist. modulus (mag)	8.76 ± 0.12	
Distance (pc)	564 ± 30	
Gaia/DR2 distance (pc)	559 ± 11	

Notes. The masses, radii, and semimajor axis a are expressed in units of the nominal solar mass and radius ($\mathcal{M}_\odot^{\rm N}$, $\mathcal{R}_\odot^{\rm N}$) as recommended by 2015 IAU Resolution B3 (see Prša et al. 2016), and the adopted solar temperature is 5772 K (2015 IAU Resolution B2). Bolometric corrections are from the work of Flower (1996), with conservative uncertainties of 0.1 mag, and the bolometric magnitude adopted for the Sun appropriate for this $\rm BC_V$ scale is $M_{\rm bol}^\odot = 4.732$ (see Torres 2010). See the text for the source of the reddening. For the apparent visual magnitude of V506 Oph out-of-eclipse, we used $V = 11.11 \pm 0.02$ (Henden & Munari 2014; Henden et al. 2015).
[a] Synchronous projected rotational velocity assuming spin–orbit alignment.
[b] Average measured projected rotational velocity from CfA and the Fairborn Observatory.

5. Light-curve Analysis

The URSA and NFO photometry of V506 Oph was analyzed using version 2013 of the Wilson–Devinney LC program (Wilson & Devinney 1971; Wilson 1979, 1990) called within a Markov chain Monte Carlo (MCMC) scheme. Our method of solution used the emcee[5] code of Foreman-Mackey et al. (2013), which is a Python implementation of the affine-invariant MCMC ensemble sampler proposed by Goodman & Weare (2010). We typically used 100 walkers and uniform priors within suitable limits for all fitted quantities.

As the system is well detached, we used the LC program in mode 2, along with the option of simple reflection and synchronous rotation of both components (see Section 6). The ephemeris and mass ratio of the binary were held fixed at the values in Table 4, and the primary temperature was set to 6840 K (Section 2). The main parameters of the fit were the inclination angle, i; the temperature of the secondary, $T_{\rm eff,2}$; the surface potentials, Φ_1 and Φ_2; a phase shift, $\Delta\phi$; and the out-of-eclipse magnitude difference at phase 0.25, m_0. We assumed initial measurement errors for the URSA and NFO observations of 0.02 mag, and a scale factor, f (with a log-uniform prior), was included as an additional adjustable parameter, which we solved for self-consistently and simultaneously with the other parameters (see Gregory 2005). Convergence of the chains was checked visually, with the additional requirement of a Gelman–Rubin statistic of 1.05 or smaller for each parameter (Gelman & Rubin 1992).

The URSA and NFO data sets were initially analyzed separately. Tests indicated the best results were obtained by solving also for the linear limb-darkening coefficients of each star (x_1, x_2), as well as the gravity-darkening exponents (β_1, β_2). More complicated limb-darkening laws did not provide any improvement. The albedos for both components were held fixed at a value of 0.5, commonly adopted for convective stars, as experiments with other values gave poorer results. No significant third light was detected, consistent with the fact that the *Gaia*/DR2 catalog (Gaia Collaboration et al. 2018) lists no companions within the photometric apertures that are bright enough to affect the light curves.

The independent URSA and NFO solutions gave similar results, so for our final solution, we solved both light curves together, imposing a common geometry as well as a single value of $T_{\rm eff,2}$ and the limb- and gravity-darkening parameters for each star, for a total of 14 free parameters. The resulting light elements are presented in Table 7, and the adopted model is shown in Figure 2 overlaid on the observations.

To guard against the possibility that the uncertainties returned by our MCMC procedure are underestimated because of residual systematic errors (i.e., time-correlated or "red" noise) in the NFO data, or even in the URSA data, we carried out a residual permutation exercise as described next. The light-curve residuals from our adopted solution were shifted by an arbitrary number of time steps (separately for URSA and NFO) and were added back into the model curve at each time of observation (with

[5] http://dfm.io/emcee/current

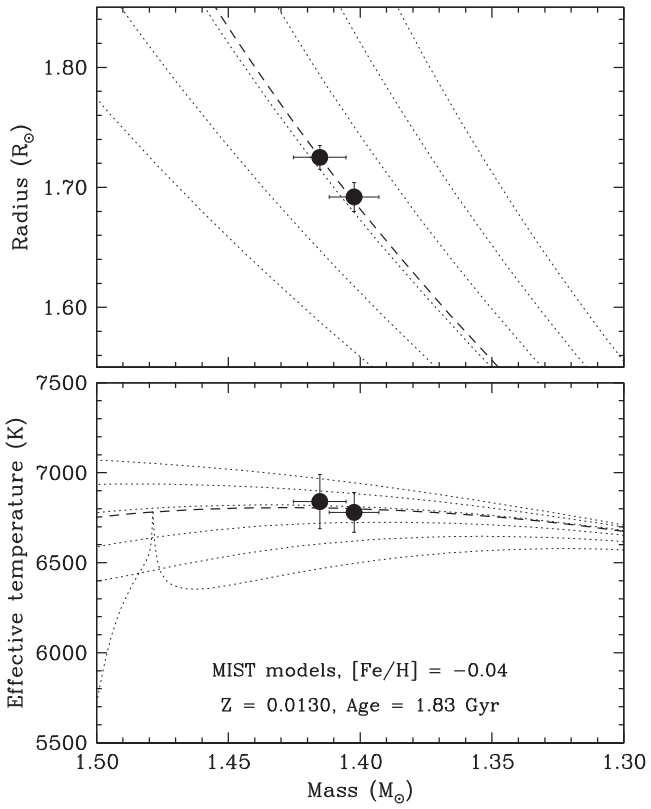

Figure 3. Mass–radius and mass–temperature diagrams for V506 Oph showing isochrones from the MIST series (Choi et al. 2016) for the best-fitting metallicity of [Fe/H] = −0.04. Dotted lines correspond to ages of 1.4–2.4 Gyr in steps of 0.2 Gyr, and the best-fit age of 1.83 Gyr is indicated with a heavier dashed line.

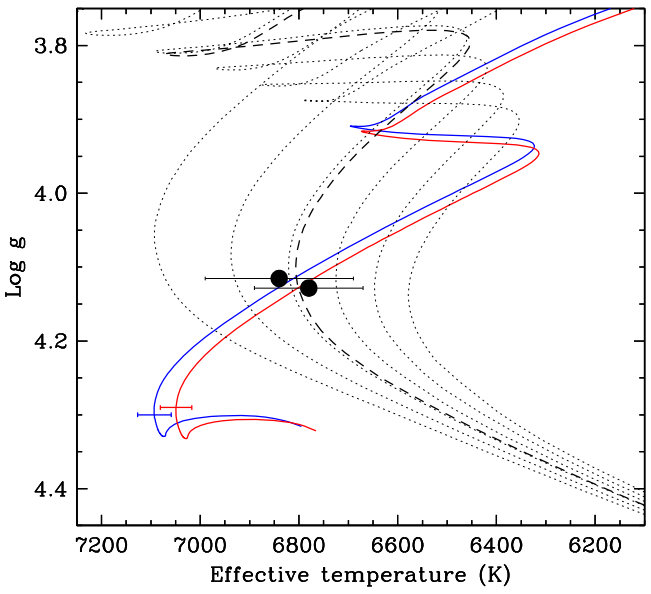

Figure 4. Evolutionary tracks for the measured masses of the V506 Oph components and [Fe/H] = −0.04. MIST isochrones (Choi et al. 2016) are shown with dotted lines for ages between 1.4 and 2.4 Gyr, as in Figure 3, with the best-fit age of 1.83 Gyr drawn as a thick dashed line. The uncertainty in the placement of the tracks that comes from the mass errors is indicated with the small error bars near the bottom of the tracks.

wrap-around) to create synthetic data sets. We subjected them to a new MCMC solution in which we simultaneously perturbed the primary temperature, the mass ratio, and the albedos by adding Gaussian noise with standard deviations equal to their reported uncertainties for $T_{\rm eff,1}$ and q, and $\sigma = 0.2$ for the albedos. We repeated this 50 times and computed the scatter (standard deviation) of the resulting distribution for each fitted and derived parameter as a measure of the uncertainty caused by red noise. We then added this uncertainty and the internal ones from the MCMC solutions in quadrature to obtain the final errors reported above in Table 7. The derived quantities include, among others, the individual Roche lobe radii as well as $r_{\rm vol}$, which is the equivalent volume radius of each star (the radius of a sphere with the same volume as the Roche lobe).

6. Absolute Dimensions

The combination of the spectroscopic elements in Table 4 and the light elements in Table 7 yields the physical properties for the system given in Table 8. The absolute masses and radii are determined with relative precisions of about 0.7% each. The averages of the measured projected rotational velocities from the CfA and Fairborn spectra agree well with the expected $v \sin i$ values for synchronous rotation (listed in the table), within the errors.

Consistent estimates of the $E(B-V)$ reddening in the direction of V506 Oph were obtained from five different sources: 0.083 (Burstein & Heiles 1982), 0.099 (Drimmel et al. 2003), 0.091 (Amôres & Lépine 2005), 0.086 (Schlafly & Finkbeiner 2011), and 0.083 (Green et al. 2018). The straight average with a conservative uncertainty is $E(B-V) = 0.088 \pm 0.020$ mag, from which the extinction is $A_V = 3.1E(B-V) = 0.273 \pm 0.062$ mag.

Using this value of A_V, the distance to the system was inferred from the radii and temperatures, the out-of-eclipse brightness of $V = 11.11 \pm 0.02$ (Henden & Munari 2014; Henden et al. 2015), and bolometric corrections from Flower (1996) and is 564 ±30 pc. This is very nearly the same as the more precise distance of 559±11 pc inferred from the *Gaia*/DR2 parallax (Gaia Collaboration et al. 2018), and the agreement speaks indirectly to the combined accuracy of our radii and effective temperatures.

As an additional check on the spectroscopic temperatures, we collected brightness measurements of the combined light of the binary from the literature in the Johnson-Cousins and Two-Micron All Sky Survey (2MASS) systems (Droege et al. 2006; Skrutskie et al. 2006; Henden & Munari 2014; Henden et al. 2015), rejecting others that are known to have been taken in an eclipse. We constructed six non-independent color indices, corrected them for reddening following Cardelli et al. (1989), and used color–temperature calibrations by Casagrande et al. (2010) to infer photometric temperatures from each index. The weighted mean of the six values, 6850±70 K, is very close to the average of the spectroscopic temperatures (6810 K), supporting the accuracy of those values. The temperature difference between the components is measured much more precisely from the light-curve analysis than from the CfA spectra and is $\Delta T_{\rm eff} = 59 \pm 24$ K.

7. Comparison with Theory

The very precise absolute dimensions of V506 Oph offer an opportunity to test current stellar evolution models. Mass–radius and mass–temperature diagrams are shown in Figure 3, in which the observations are compared against model isochrones from the MESA Isochrones and Stellar Tracks series (MIST; Choi et al. 2016), which is based on the Modules for Experiments in Stellar Astrophysics package (MESA; Paxton et al. 2011, 2013, 2015). To

our knowledge, there is no spectroscopic determination available for the metallicity of V506 Oph. We find that a slight adjustment in the metallicity of the models from solar to [Fe/H] = −0.04 provides an excellent fit to both radii and both effective temperatures at the measured masses. The age of the system according to these models is 1.83 Gyr, which is shown by the thick dashed line in Figure 3.

Evolutionary tracks for the measured masses are seen in Figure 4, and indicate the components are halfway through their main-sequence lifetimes. The uncertainty in the location of the tracks due to the mass errors is shown at the bottom and corresponds to only about ±30 K in this diagram.

8. Discussion

V506 Oph has been listed as a possible member of the sparse open cluster Collinder 359 (Melotte 186; Sahade & Frieboes 1960; Sahade & Berón Dàvila 1963), although the location of the binary nearly 7° from the cluster center makes this rather unlikely a priori. Curiously, many of the V506 Oph properties appear consistent with this membership. For example, the recent study by Cantat-Gaudin et al. (2018) listed the parallax of Collinder 359 as $\pi = 1.93 \pm 0.10$ mas, corresponding to a distance of about 520 ±27 pc, which is consistent with what we obtain for the binary (564±31 pc; Table 8). Kharchenko et al. (2005) reported the mean radial velocity of the cluster to be -4.45 ± 0.25 km s^{-1}, though based on measurements for only two stars. This is also tantalizingly close to the center-of-mass velocity we measured for V506 Oph, -3.88 ± 0.43 km s^{-1}. The mean proper motion components of Collinder 359 listed by Cantat-Gaudin et al. (2018) are $\mu_\alpha \cos\delta = +1.98 \pm 0.23$ mas yr^{-1} and $\mu_\delta = -8.19 \pm 0.25$ mas yr^{-1} based on the Fourth U.S. Naval Observatory CCD Astrograph Catalog (UCAC4; Zacharias et al. 2013). Those of V506 Oph in the same catalog are $\mu_\alpha \cos\delta = -1.8 \pm 1.4$ mas yr^{-1} and $\mu_\delta = -4.9 \pm 1.5$ mas yr^{-1}, which differ at about the 2.5σ level from the cluster mean. However, if the ∼30 Myr age of Collinder 359 reported by Kharchenko et al. (2005) is accurate, then V506 Oph cannot be a member, as we find it to be much older (1.83 Gyr).

V506 Oph joins the ranks of the detached eclipsing binaries with the very best determined properties (see, e.g., Torres et al. 2010). Its value for testing models of stellar evolution would be significantly enhanced by a spectroscopic determination of the metallicity, although this may be challenging given the significant line broadening of both stars.

We are grateful to the observers P. Berlind, M. Calkins, and G. Esquerdo for their assistance in obtaining the CfA spectra. J. Mink is also acknowledged for maintaining the CfA echelle database. The anonymous referee provided helpful comments that improved the original manuscript. The authors wish to thank Bill Neely, who operates and maintains the NFO WebScope for the Consortium and who handles preliminary processing of the images and their distribution. G.T. acknowledges partial support from the NSF through grant AST-1509375. Astronomy at Tennessee State University is supported by the state of Tennessee through its Centers of Excellence Program. The computational resources used for this research include the Smithsonian Institution's "Hydra" High Performance Cluster. This research has made use of the SIMBAD database and the VizieR catalog access tool, both operated at the CDS, Strasbourg, France, and of NASA's Astrophysics Data System Abstract Service. This work has also made use of data from the European Space Agency (ESA) mission *Gaia* (https://www.cosmos.esa.int/gaia), processed by the *Gaia* Data Processing and Analysis Consortium (DPAC, https://www.cosmos.esa.int/web/gaia/dpac/consortium). Funding for the DPAC has been provided by national institutions, in particular the institutions participating in the *Gaia* Multilateral Agreement.

ORCID iDs

Guillermo Torres https://orcid.org/0000-0002-5286-0251
Claud H. Sandberg Lacy https://orcid.org/0000-0002-0455-679X
Francis C. Fekel https://orcid.org/0000-0002-9413-3896

References

Amôres, E. B., & Lépine, J. R. D. 2005, AJ, 130, 659
Burstein, D., & Heiles, C. 1982, AJ, 87, 1165
Cantat-Gaudin, T., Vallenari, A., Sordo, R., et al. 2018, A&A, 615, A49
Cardelli, J. A., Clayton, G. C., & Mathis, J. S. 1989, ApJ, 345, 245
Casagrande, L., Ramírez, I., Meléndez, J., Bessell, M., & Asplund, M. 2010, A&A, 512, A54
Choi, J., Dotter, A., Conroy, C., et al. 2016, ApJ, 823, 102
Drimmel, R., Cabrera-Lavers, A., & López-Corredoira, M. 2003, A&A, 409, 205
Droege, T. F., Richmond, M. W., Sallman, M. P., & Creager, R. P. 2006, PASP, 118, 1666
Eaton, J. A., & Williamson, M. H. 2007, PASP, 119, 886
Fekel, F. C., Rajabi, S., Muterspaugh, M. W., & Williamson, M. H. 2013, AJ, 145, 111
Fekel, F. C., Tomkin, J., & Williamson, M. H. 2009, AJ, 137, 3900
Flower, P. J. 1996, ApJ, 469, 355
Foreman-Mackey, D., Hogg, D. W., Lang, D., & Goodman, J. 2013, PASP, 125, 306
Fűrész, G. 2008, PhD thesis, Univ. Szeged, Hungary
Gaia Collaboration, Brown, A. G. A., Vallenari, A., et al. 2018, A&A, 616, A1
Gelman, A., & Rubin, D. B. 1992, StaSc, 7, 457
Goodman, J., & Weare, J. 2010, Commun. Appl. Math. Comput. Sci., 5, 65
Green, G. M., Schlafly, E. F., Finkbeiner, D., et al. 2018, MNRAS, 478, 651
Gregory, P. C. 2005, ApJ, 631, 1198
Henden, A., & Munari, U. 2014, CoSka, 43, 518
Henden, A. A., Levine, S., Terrell, D., & Welch, D. L. 2015, AAS Meeting, 225, 336.16
Hoffmeister, C. 1935, AN, 255, 401
Kharchenko, N. V., Piskunov, A. E., Röser, S., Schilbach, E., & Scholz, R.-D. 2005, A&A, 438, 1163
Kochanek, C. S., Shappee, B. J., Stanek, K. Z., et al. 2017, PASP, 129, 104502
Lacy, C. H. S. 2007, IBVS, 5764, 1
Lacy, C. H. S., Torres, G., Fekel, F. C., & Mutterspaugh, M. W. 2014, AJ, 147, 148
Lapham, J., & Snyder, L. F. 2007, in Society for Astronomical Sciences Annual Symp. 26, ed. B. D. Warner et al. (Rancho Cucamonga, CA: SAS), 141
Latham, D. W., Stefanik, R. P., Torres, G., et al. 2002, AJ, 124, 1144
Nordström, B., Latham, D. W., Morse, J. A., et al. 1994, A&A, 287, 33
Paxton, B., Bildsten, L., Dotter, A., et al. 2011, ApJS, 192, 3
Paxton, B., Cantiello, M., Arras, P., et al. 2013, ApJS, 208, 4
Paxton, B., Marchant, P., Schwab, J., et al. 2015, ApJS, 220, 15
Pojmanski, G., & Maciejewski, G. 2004, AcA, 54, 153
Prša, A., Harmanec, P., Torres, G., et al. 2016, AJ, 152, 41
Sahade, J., & Berón Dàvila, F. 1963, AnAp, 26, 153
Sahade, J., & Frieboes, H. 1960, PASP, 72, 52
Sandberg Lacy, C. H., & Fekel, F. C. 2011, AJ, 142, 185
Scarfe, C. D. 2010, Obs, 130, 214
Schlafly, E. F., & Finkbeiner, D. P. 2011, ApJ, 737, 103
Skrutskie, M. F., Cutri, R. M., Stiening, R., et al. 2006, AJ, 131, 1163
Soloviev, A. 1937, Tadjik Obs. Circ., 22, 3
Szentgyorgyi, A. H., & Fűrész, G. 2007, RMxAC, 28, 129
Torres, G. 2010, AJ, 140, 1158
Torres, G., Andersen, J., & Giménez, A. 2010, A&ARv, 18, 67
Torres, G., Neuhäuser, R., & Guenther, E. W. 2002, AJ, 123, 1701
Wilson, R. E. 1979, ApJ, 234, 1054
Wilson, R. E. 1990, ApJ, 356, 613
Wilson, R. E., & Devinney, E. J. 1971, ApJ, 166, 605
Zacharias, N., Finch, C. T., Girard, T. M., et al. 2013, AJ, 145, 44
Zucker, S., & Mazeh, T. 1994, ApJ, 420, 806